J. Fluid Mech. (1987), *vol.* 179, *pp.* 307–326
Printed in Great Britain

Turbulent energy dissipation in a wake

By L. W. B. BROWNE, R. A. ANTONIA AND D. A. SHAH
Department of Mechanical Engineering, University of Newcastle, NSW 2308, Australia

(Received 30 April 1986 and in revised form 5 November 1986)

The average turbulent energy dissipation is often estimated by assuming isotropy and measuring the temporal derivative of the longitudinal velocity fluctuation. In this paper, the nine major terms that make up the total dissipation have been measured in the self-preserving region of a cylinder wake for a small turbulence Reynolds number. The results indicate that local isotropy is not satisfied; the isotropic dissipation, computed by assuming isotropic relations, being smaller than the total dissipation by about 45% on the wake centreline and by about 80% near the wake edge. Indirect verification of the dissipation measurements is provided by the budget of the turbulent kinetic energy. This budget leads to a plausible distribution for the pressure diffusion term, obtained by difference.

1. Introduction

In many of the computer approaches that are used to calculate turbulent flows, the average turbulent energy dissipation is estimated by assuming isotropy and measuring the temporal derivative of the longitudinal velocity fluctuation. The energy dissipation is a significant term in the governing equations used in the calculations and it is therefore important that accurate estimates for this term be available. In this paper we present measurements of the nine major terms that make up the total dissipation in the self-preserving region of a cylinder wake.

The total average turbulent energy dissipation $\bar{\epsilon}$ is given by (e.g. Hinze 1975 p. 218)

$$\bar{\epsilon} = \nu \overline{\left(\frac{\partial u_i}{\partial x_j} + \frac{\partial u_j}{\partial x_i}\right) \frac{\partial u_j}{\partial x_i}}, \tag{1}$$

using standard Cartesian tensor notation and summation on repeated indices. The isotropic value $\bar{\epsilon}_I$ of $\bar{\epsilon}$, first obtained by Taylor (1935), can be economically derived from the isotropic relation†

$$\overline{\left(\frac{\partial u_i}{\partial x_j}\right)\left(\frac{\partial u_k}{\partial x_m}\right)} = \frac{1}{2}\overline{\left(\frac{\partial u_1}{\partial x_1}\right)^2}(4\delta_{ik}\delta_{jm} - \delta_{ij}\delta_{km} - \delta_{im}\delta_{jk}), \tag{2}$$

where $\delta_{\alpha\beta}$ is the Kronecker delta ($\delta_{\alpha\beta} = 1$ if $\alpha = \beta$, $= 0$ if $\alpha \neq \beta$). Using (1), (2) and the more usual notation for velocity fluctuations and coordinate axes (u, v, w instead of u_1, u_2, u_3 and x, y, z instead of x_1, x_2, x_3)

$$\bar{\epsilon}_I = 15\nu\overline{\left(\frac{\partial u}{\partial x}\right)^2}. \tag{3}$$

† This follows from the isotropic fourth-order tensor expression (e.g. Jeffreys 1963) using symmetry and continuity.

The total dissipation ϵ contains 12 terms,

$$\bar{\epsilon} = \nu\Big\{\underbrace{2\overline{\left(\frac{\partial u}{\partial x}\right)^2}}_{[1]} + \underbrace{\overline{\left(\frac{\partial v}{\partial x}\right)^2}}_{[2]} + \underbrace{\overline{\left(\frac{\partial w}{\partial x}\right)^2}}_{[3]} + \underbrace{\overline{\left(\frac{\partial u}{\partial y}\right)^2}}_{[4]} + \underbrace{2\overline{\left(\frac{\partial v}{\partial y}\right)^2}}_{[5]} + \underbrace{\overline{\left(\frac{\partial w}{\partial y}\right)^2}}_{[6]} + \underbrace{\overline{\left(\frac{\partial u}{\partial z}\right)^2}}_{[7]} + \underbrace{\overline{\left(\frac{\partial v}{\partial z}\right)^2}}_{[8]}$$
$$+ \underbrace{2\overline{\left(\frac{\partial w}{\partial z}\right)^2}}_{[9]} + \underbrace{2\overline{\left(\frac{\partial u}{\partial y}\right)\left(\frac{\partial v}{\partial x}\right)}}_{[10]} + \underbrace{2\overline{\left(\frac{\partial u}{\partial z}\right)\left(\frac{\partial w}{\partial x}\right)}}_{[11]} + \underbrace{2\overline{\left(\frac{\partial v}{\partial z}\right)\left(\frac{\partial w}{\partial y}\right)}}_{[12]}\Big\}. \quad (4)$$

For isotropy, the first 9 terms are equal and using (2), terms [10], [11] and [12] are negative and of half the magnitude of the other terms, viz.

$$\overline{\left(\frac{\partial u}{\partial y}\right)\left(\frac{\partial v}{\partial x}\right)} = \overline{\left(\frac{\partial u}{\partial z}\right)\left(\frac{\partial w}{\partial x}\right)} = \overline{\left(\frac{\partial v}{\partial z}\right)\left(\frac{\partial w}{\partial y}\right)} = -\frac{1}{2}\overline{\left(\frac{\partial u}{\partial x}\right)^2}. \quad (5)$$

The assumption of isotropy can be directly checked by measuring the 12 terms of (4). As far as we know, the greatest number of terms that have been measured in the laboratory is five (terms [1], [2], [3], [4] and [7] by Laufer 1954; Wygnanski & Fiedler 1969 and by Verollet 1972).

The easiest quantities to measure are $\overline{(\partial u/\partial x)^2}$, $\overline{(\partial v/\partial x)^2}$ and $\overline{(\partial w/\partial x)^2}$ since they can be derived from temporal derivatives of u, v, w using Taylor's hypothesis ($\partial/\partial x \equiv -\overline{U}^{-1}\partial/\partial t$, where $\overline{U}$ is the local mean velocity). Term 1 can be obtained from a single hot wire while the other two require one X-wire. Several published values of the ratios K_1 and K_2, where

$$K_1 = 2\overline{\left(\frac{\partial u}{\partial x}\right)^2}\Big/\overline{\left(\frac{\partial v}{\partial x}\right)^2}, \quad (6)$$

and

$$K_2 = 2\overline{\left(\frac{\partial u}{\partial x}\right)^2}\Big/\overline{\left(\frac{\partial w}{\partial x}\right)^2}, \quad (7)$$

are shown in table 1 for various turbulent shear flows. For isotropy K_1 and K_2 should be 1.0. The majority of entries in this table indicate that K_1 and K_2 do not satisfy isotropy. Although K_1 and K_2 are approximately equal, their magnitudes are generally greater than 1.0.

The quantities $\overline{(\partial u/\partial y)^2}$ and $\overline{(\partial u/\partial z)^2}$ are also measurable. They can be obtained using two parallel hot wires and techniques that are described later, provided several possible sources of error are taken into account (e.g. Antonia & Browne 1986, hereinafter referred to as I). There are fewer published measurements for $\overline{(\partial u/\partial y)^2}$ and $\overline{(\partial u/\partial z)^2}$ compared with those for terms [1], [2] and [3]. This is evident in table 2 which reports values of the ratios K_3 and K_4, where

$$K_3 = 2\overline{\left(\frac{\partial u}{\partial x}\right)^2}\Big/\overline{\left(\frac{\partial u}{\partial y}\right)^2}, \quad (8)$$

and

$$K_4 = 2\overline{\left(\frac{\partial u}{\partial x}\right)^2}\Big/\overline{\left(\frac{\partial u}{\partial z}\right)^2}. \quad (9)$$

For isotropy, K_3 and K_4 should be 1.0. The results in table 2 suggest that although K_3 and K_4 are nearly equal, their magnitude is consistently smaller than 1.0.

The quantities

$$\overline{(\partial v/\partial y)^2},\ \overline{(\partial w/\partial y)^2},\ \overline{(\partial v/\partial z)^2},\ \overline{(\partial w/\partial z)^2},\ \overline{(\partial u/\partial y)(\partial v/\partial x)} \quad \text{and} \quad \overline{(\partial u/\partial z)(\partial w/\partial x)}$$

Flow	Experimental details		K_1	K_2	Reference
Quasi-homogeneous shear flow	$R_\lambda = 160$		1.30	1.30	Tavoularis & Corrsin (1981)
Boundary layer	$R_\delta \approx 50000$	$y/\delta \approx 0.08$	1.65	1.57	Verollet (1972)
		≈ 0.32	1.72	1.59	
Pipe	$R_d = 50000$	Near wall	3.3	1.8	Laufer (1954)
		Half radius	1.0	0.83	
	$= 500000$	Near wall	1.73	1.73	
		Half radius	1.40	1.12	
	$= 90000$	Near wall	1.22	1.22	Lawn (1971)
		Half radius	1.27	1.27	
Circular jet	$R_d = 100000$	$y/x = 0$	0.98	0.98	Wygnanski & Fiedler (1969)
		$= 0.05$	1.25	1.25	
		$= 0.1$	1.75	1.75	
Plane jet (without external flow)	$R_\lambda = 990$	$y/x = 0$	1.47	1.47	Gutmark & Wygnanski (1976)
		$= 0.05$	1.59	1.59	
		$= 0.1$	1.77	1.77	
	$R_\lambda = 204$	Centreline	1.32	1.32	Antonia *et al.* (1982)
	$R_\lambda = 300$	Centreline	1.33	1.33	Everitt & Robins
	$= 200$	Halfwidth	2.0	2.0	(1978)
Plane jet (with external flow)	Strong jet	Centreline	1.82	1.82	Everitt & Robins (1978)
		Halfwidth	2.0	2.0	
	Weak jet	Centreline	1.18	1.54	
		Halfwidth	1.18	1.33	
Mixing layer	$R_\lambda = 330$		1.74	—	Champagne *et al.* (1976)
Two-dimensional cylinder wake	$R_d = 2700$	$y/d = 0$	0.99	1.23	Fabris (1974)
		$= 6$	1.15	1.25	
	$R_d = 19050$	$y/d = 0$	1.16	1.12	Champagne (1978)
	$R_d = 8400$	across the wake	1.0	1.0	Townsend (1948)

Note: $R_\lambda = \overline{u^2}^{\frac{1}{2}}\lambda/\nu$ where $\lambda = [\overline{u^2}/\overline{(\partial u/\partial x)^2}]^{\frac{1}{2}}$.

TABLE 1. Ratios K_1 and K_2

require the use of two X-wires very close together. Values of these quantities have not been reported in the literature. The term $\overline{(\partial v/\partial z)(\partial w/\partial y)}$ which requires four X-wires (or two 3-wire probes) would be too difficult to measure with any reasonable accuracy. We focus attention on the first nine terms in (4). Term [12] was not measured and, while an attempt was made to estimate terms [10] and [11], the accuracy of these terms was poor. This is considered further in §4.

In I, measurements were made of all three components of the average temperature dissipation in the self-preserving region of a turbulent wake for the same experimental conditions as used here. These measurements, supported by a satisfactory closure of the temperature variance budget, indicated that the dissipation is larger than the isotropic value by about 50% near the wake centreline and almost 100% near the region of maximum production. It was therefore important to ascertain whether a similar magnitude of departure from isotropy occurred for the average turbulent energy dissipation. The existence of such a departure is not immediately evident from the results in tables 1 and 2 since opposite trends $K_1 \approx K_2 > 1$ (table 1) and

Flow	Experimental details		K_3†	K_4†	Reference
Boundary layer	$R_\delta = 50000$	$y/\delta \approx 0.08$	0.76	0.80	Verollet (1972)
		≈ 0.32	0.76	0.78	
Pipe	$R_d = 50000$	Near wall	0.40	0.40	Laufer (1954)
		At half radius	0.69	0.56	
	$= 500000$	Near wall	0.93	0.93	
		At half radius	0.80	0.80	
	$R_d = 90000$	Across pipe	1.0	—	Lawn (1971)
Circular jet	$R_d = 100000$	$y/x = 0$	1.2	1.2	Wygnanski & Fiedler (1969)
		$= 0.05$	0.83	0.83	
		$= 0.1$	0.32	0.32	
Plane jet (without external flow)	$R_\lambda = 204$	Jet centreline	0.57	—	Antonia *et al.* (1984)

† The cylindrical coordinate equivalent is used for pipe flows.

TABLE 2. Ratios K_3 and K_4

$K_3 \approx K_4 < 1$ (table 2) suggest the possibility of a compensation between different terms in (4) and therefore the possibility that (3) may be a reasonable approximation to (4).

An important advantage of the experimental conditions we use here is the relatively large size of the Kolmogorov microscale $L_K\,[\equiv (\nu^3/\bar{\epsilon})^{\frac{1}{4}}]$, ranging from about 0.45 mm† near the centreline to about 0.9 mm† near the edge of the wake. Such a range imposes only a small spatial resolution constraint on the measurement of velocity derivatives using two X-probes. It may be claimed that a disadvantage of our experimental conditions is the small value of the turbulence Reynolds number, defined by $R_\lambda = \overline{u^2}^{\frac{1}{2}}\lambda/\nu$, where $\lambda = (\overline{u^2}/\overline{(\partial u/\partial x)^2})^{\frac{1}{2}}$ is the Taylor microscale. In the present flow $R_\lambda \approx 40$ at the centreline and $R_\lambda \approx 80$ near the edge. However, there is little evidence to suggest that departures from local isotropy decrease with increasing Reynolds number (e.g. tables 1 and 2) so that, as pointed out by Nelkin & Nakano (1984) and Antonia, Anselmet & Chambers (1986), it is important to document departures from local isotropy at laboratory values of R_λ. In the context of the average dissipation of turbulent energy (or of the temperature variance) the independence of the anisotropy with Reynolds number may be a consequence of the anisotropic large-scale structures of the flow.

In this paper, we report measurements of the nine major terms in (4) for the same location and experimental conditions as used in I. Experimental details are given in §2 and the accuracy of the data is briefly discussed in §3. The main results are presented and discussed in §4. The accuracy of these results is indirectly considered in §5 in the context of the budget, for the average turbulent kinetic energy. A brief comparison is given in §6 between the average dissipation of turbulent energy and the average dissipation of the temperature variance which was presented in I.

† These estimates are based on ϵ_1. The values of ϵ reported later in this paper indicate that these estimates should be smaller by about 10%.

2. Experimental details

Measurements were made in the working section (350 mm × 350 mm, 2.4 m long) of an open return type wind tunnel. A stainless steel tube of diameter $d = 2.67$ mm was mounted in the midplane of the working section, normal to the flow and 20 cm after the end of the contraction leading into the working section. The free-stream velocity U_1 was 6.7 m/s so that the Reynolds number R_d based on the cylinder diameter was 1170. The floor of the working section was slightly tilted to produce a zero pressure gradient and all measurements were made at $x/d = 420$. Full details of the experimental set-up are given in I.

Three types of measurements were used:

1. Single hot wires and single X-wires. Single hot wires allow measurements of $\overline{(\partial u/\partial x)^2}$ while, depending on their orientation, single X-wires allow measurements of $\overline{(\partial u/\partial x)^2}$ and $\overline{(\partial v/\partial x)^2}$ or $\overline{(\partial u/\partial x)^2}$ and $\overline{(\partial w/\partial x)^2}$. These measurements were made over a period of time, before the current measurements, in connection with other studies of the cylinder wake. They are used here for measurement verification, i.e. the corresponding values obtained from the current experiments can be compared with these previously obtained values.

2. Two single hot wires to obtain $\overline{(\partial u/\partial y)^2}$ and $\overline{(\partial u/\partial z)^2}$. Since measurement techniques using two single hot wires have been well investigated (see discussion below), it was expected that the measurements would provide an important verification of similar quantities obtained using two X-wires.

3. Two X-wires to obtain terms [1] to [11] of (4).

Measurements of type 2 were carried out with hot wires (Pt–10 % Rh) of length $l_w \approx 0.8$ mm and diameter $d_w = 5$ μm. The wires were located at the same x-position and parallel to the cylinder. For the y-derivatives the wires were located centrally in the duct and at the same z-position. The distance between them was varied from 0.2 mm to 3.8 mm to allow an estimate to be made of $\overline{(\partial u/\partial y)^2}$ using the difference technique (Antonia, Browne & Chambers 1984) and the correlation technique (Taylor 1935; Verollet 1972; Antonia *et al.* 1984; I; Krishnamoorthy & Antonia 1987). A summary of these techniques is given later. For the z-derivatives the wires were separated in the y-direction by 0.2 mm and then the z-separation was varied from 0.2 mm to 3.8 mm so that again the difference and the correlation techniques could be used to estimate $\overline{(\partial u/\partial z)^2}$.

Measurements of type 3 were carried out with standard TSI X-probes, tungsten wires with $d_w = 5$ μm and $l_w \approx 1.2$ mm. The physical arrangements of the two X-wires are shown in figure 1. Note that some of the terms in (4) were measured a number of times with these arrangements.

The hot wires were operated with in-house and DISA 55M10 constant temperature circuits at an overheat ratio of 0.6. The frequency response of the circuits, determined by the square-wave technique, extended to about 20 kHz. Output voltages from the anemometers were passed through buck and gain circuits and low-pass filtered (Krohn–Hite model 3323) at a frequency equal to 2.4 kHz. This latter value was chosen to correspond approximately to the Kolmogorov frequency, f_K, ($f_K = \overline{U}/2\pi L_K$) at the centreline. As indicated previously, the Kolmogorov microscale, L_K, increases away from centreline by a factor of about two. Thus the low-pass filter frequency, f_c, was almost twice the local Kolmogorov frequency near the edge of the wake. The filtered signals were subsequently sampled at a frequency equal to $2f_c$ into a PDP 11/34 computer using an 11 bit plus sign A/D converter. Yaw and

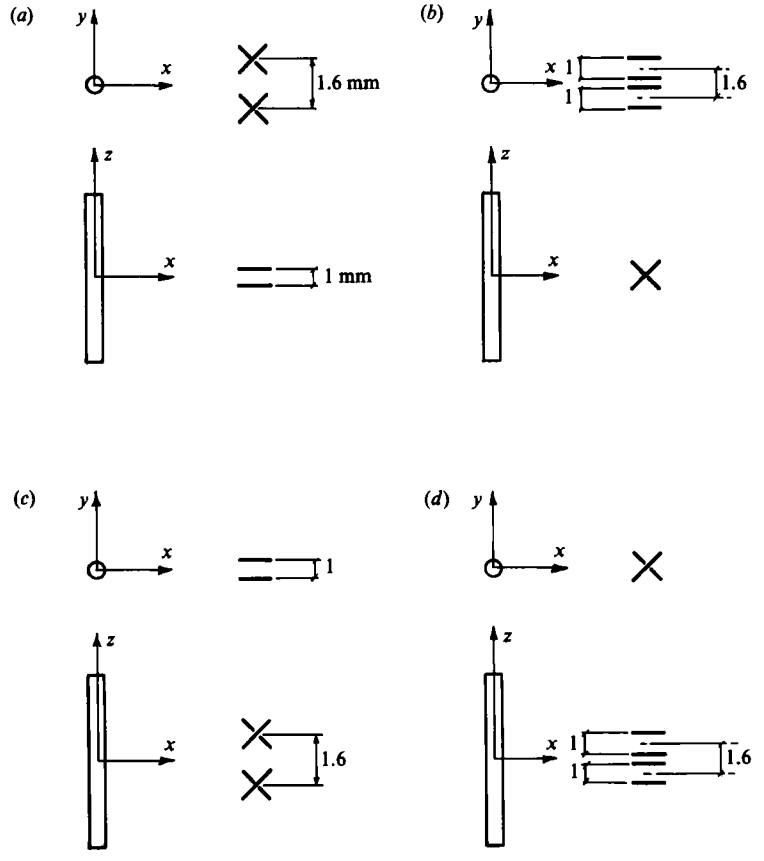

FIGURE 1. Illustration of the coordinate system used and the experimental arrangement of the two X-probes. (*a*) for terms [1], [2], [4], [5], [10] of (4); (*b*) [1], [3], [4], [6]; (*c*) [1], [3], [7], [9], [11]; (*d*) [1], [2], [7], [8].

velocity calibrations were carried out using a data logger and personal computer combination.

Measurements were made at a number of y-positions across the flow, from $y = 0$ to $y = 25$ mm. Normalization of y is by L, the position of y where the velocity defect is half its centreline value, i.e. $\eta = y/L$. At the measurement station, $L = 12.3$ mm.

3. Some checks of measurement accuracy

Before presenting results for the velocity derivatives, we briefly consider here some of the checks that were made to ensure the reliability of the data.

From all measurements, a large number of $\overline{u^{2\frac{1}{2}}}$, $\overline{v^{2\frac{1}{2}}}$ and $\overline{w^{2\frac{1}{2}}}$ values were obtained. Most of these are shown in figure 2 but not all the results for $\overline{u^{2\frac{1}{2}}}$ are shown. The results left out do not change the picture. It is interesting to note, in common with many turbulence measurements, any one set of measurements tend to lie on a curve but the curves from one experiment to another are not the same. Best-fit curves to the data, from measurements of types 1, 2 and 3, have been drawn as well as the bars that cover the scatter of data from all measurements. The r.m.s. error bars would be less than the scatter bars. In general, single X-wire results for $\overline{u^{2\frac{1}{2}}}$ were satisfactorily close

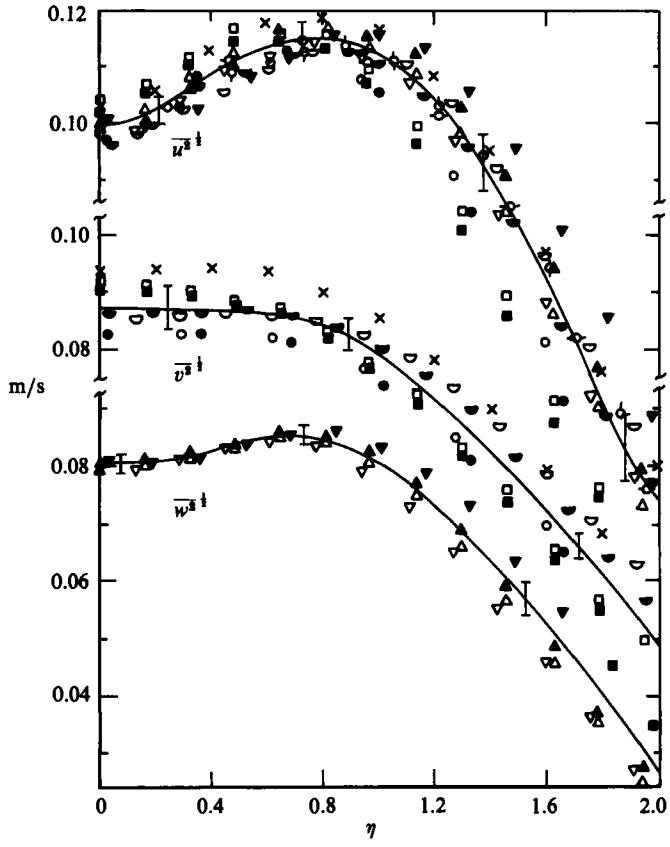

FIGURE 2. Distribution across the wake of the r.m.s. of the turbulent velocity fluctuations. ○, lower X-wire; ●, upper X-wire of figure 1 (*a*); ⌓, lower X-wire; ⌣, upper X-wire of figure 1 (*a*) (repeated); ▽, lower X-wire; ▼, upper X-wire of figure 1 (*b*); △, X-wire at $z = 0$; ▲, X-wire at $z = 1.6$ mm in figure 1 (*c*); □, X-wire at $z = 0$; ■, X-wire at $z = 1.6$ mm in figure 1 (*d*); ×, single X-wire (previous experiments); –○–, single hot wire (previous experiments); ◇, single hot wire (previous experiments).

to those obtained with a single hot wire. Also, results for $\overline{u^2}^{\frac{1}{2}}, \overline{v^2}^{\frac{1}{2}}, \overline{w^2}^{\frac{1}{2}}$ obtained with two X-wires were in good agreement with those obtained with a single X-wire. This indicated that little interference occurred between the X-wires.

There are several sources of uncertainty associated with the measurement of derivatives, especially those involving the use of two hot wires. A full discussion of these is in Antonia *et al.* (1986). Here the following criteria were considered:

(i) Spatial resolution: the diameter, d_w, and length, l_w, of the hot wires were chosen so that the ratio of wire length to the Kolmogorov microscale, l_w/L_K was as small as practicable, while l_w/d_w was large enough to ensure that end conduction errors were negligible. For single hot wires, $l_w/d_w \approx 150$ and l_w/L_K varied from 0.8 at the edge of the wake to 1.7 at the wake centreline. For the two X-wire measurements, the corresponding values were 250 and $l_w/L_K \approx 1.3$ to 2.7. The l_w/d_w ratios used for the present measurements are close to the generally accepted value of 200 (Champagne 1978). For the present maximum values of l_w/L_K and wavenumber, the hot-wire length corrections of Wyngaard (1968) indicate that the measured one-dimensional spectrum is underestimated by an amount which increases, as the

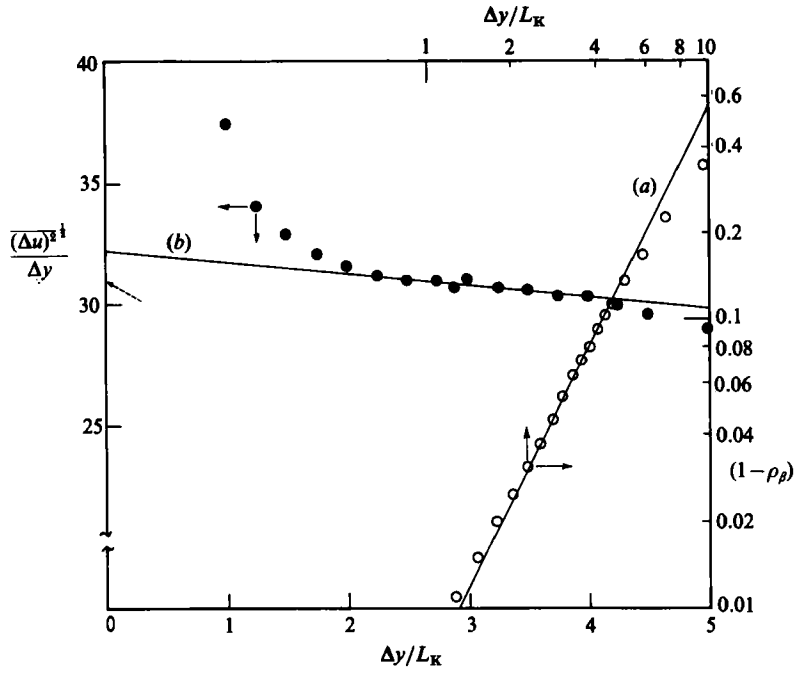

FIGURE 3. (*a*) Log–log representation of $(1-\rho_\beta)$ as a function of $\Delta y/L_K$. ○, $\eta = 0.8$. ——, line of slope 2. (*b*) Dependence of $\overline{(\Delta u)^2}^{\frac{1}{2}}/\Delta y$ on $\Delta y/L_K$. ●, $\eta = 0.8$. ——, linear extrapolation of data for $\Delta y/L_K > 2.0$. Arrow (–––→) indicates value obtained from correlation technique.

wavenumber increases, to a maximum of about 14%. This correction is comparable to the experimental scatter and therefore wire length corrections were not applied.

(ii) Cut-off frequency f_c of the low-pass filter: the correct selection of this frequency is important for fine-scale turbulence studies (Champagne 1978; Antonia *et al.* 1986). For the present measurements, the skewness S and flatness factor F of $\partial u/\partial x$ were approximately constant for $f_c \geqslant f_K$, where f_K is the Kolmogorov frequency, indicating that the selection of $f_c \geqslant f_K$ was satisfactory.

(iii) Frequency response of the instruments and the record duration for each measurement: both of these were sufficient to ensure, as required (Antonia *et al.* 1986), closure of the tails of the probability density functions of all temporal and spatial derivatives and good convergence for the moments of interest.

As noted in §2, type 2 measurements were made to provide a basis for comparison with the more difficult type 3 measurements. The gradients $\overline{(\partial u/\partial y)^2}$ and $\overline{(\partial u/\partial z)^2}$ were obtained from: (*a*) a two-point correlation technique, and (*b*) the difference between velocity fluctuations at two points. A description of these two methods was given in I and is presented in summary form here.

Let $\beta_1(t)$ and $\beta_2(t)$ be the data for turbulence quantity β recorded simultaneously at two points in space, 1 and 2. Then the autocorrelation of the two signals is defined by

$$\rho_\beta = \overline{\beta_1(t)\,\beta_2(t)}/\overline{\beta_1^2}^{\frac{1}{2}}\,\overline{\beta_2^2}^{\frac{1}{2}}. \tag{10}$$

If the points are separated by a small distance p in any arbitrary direction r, then ρ_β can be approximated (Batchelor 1953 p. 47), to order p^4, by

$$\rho_\beta \approx 1 - p^2\overline{(\partial\beta/\partial r)^2}/2\overline{\beta^2}, \tag{11}$$

where $\overline{\beta^2}$ can be calculated using $\frac{1}{2}(\overline{\beta_1^2}+\overline{\beta_2^2})$. From (11)

$$\overline{\left(\frac{\partial\beta}{\partial r}\right)^2} \approx 2\overline{\beta^2}\frac{(1-\rho_\beta)}{p^2} \tag{12}$$

and ρ_β can be obtained from (10).

This approach for estimating the derivative is known as the correlation technique. If (12) is plotted on $(1-\rho_\beta)$ *vs.* p-axis, using log–log scales, a line of slope 2 is obtained. Such a line can therefore be used, figure 3(*a*), to determine which range of experimental points best satisfies (12). (In figure 3(*a*), $u \equiv \beta$, $y \equiv r$ and $\Delta y \equiv p$). Any point on the line can then be used in (12) to estimate the derivative.

In the difference technique for estimating the derivatives, use is made of

$$\frac{\partial\beta}{\partial r} \approx \frac{(\beta_2-\beta_1)}{p}. \tag{13}$$

This, theoretically, becomes more accurate as $p \to 0$. In figure 3(*b*), where $\Delta y \equiv p$ and $\Delta u \equiv \beta_2-\beta_1$, the experimental points, obtained using (13), show that an extrapolation procedure has to be used to estimate the derivative as $\Delta y \to 0$. The reason for this is the large relative errors in $\beta_2-\beta_1$ and in p that apply to the measurements for very small separations.

At $\eta = 0.8$, the correlation technique (figure 3*a*) yields a value for $\overline{(\partial u/\partial y)^2}^{\frac{1}{2}}$ of 31 s^{-1} while the difference technique (figure 3*b*) yields 32 s^{-1} when data in the range $2 < \Delta y/L_K < 4$ are extrapolated to zero separation. The difference technique is easier to apply and it was used with the two X-wires: at $\eta = 0.8$, $\overline{(\partial u/\partial y)^2}^{\frac{1}{2}} \approx 32$ s^{-1} with $\Delta y/L_K \approx 3.4$. This value is only slightly larger than the value of $\overline{(\partial u/\partial y)^2}^{\frac{1}{2}}$ inferred from figure 3(*b*) for a corresponding separation. In view of the uncertainty in the linear extrapolation in figure 3(*b*), we have chosen not to correct our two X-wires results for the finite separation (1.6 mm) between sensors. The level of agreement for $\overline{(\partial u/\partial y)^2}^{\frac{1}{2}}$ (within 9%) and $\overline{(\partial u/\partial z)^2}^{\frac{1}{2}}$ (within 15%) using either two single wires or two X-wires indicated that reliable estimates can be obtained using two X-wires.

4. Results for mean-square derivatives

The experimental values obtained for the r.m.s. of the derivatives, $\overline{(\partial u_i/\partial x_j)^2}^{\frac{1}{2}}$ [with no summation on i and j], are shown in figure 4. Terms are represented by their best-fit curve and error bars. The experimental scatter is generally within $\pm 5\%$ near the centreline, increasing to $\pm 10\%$ near the edge of the wake. It should be noted that the values obtained were approximately the same for the three types of measurements.

Using the data shown in figure 4, terms [1] to [9] of (4) were determined and the results are plotted in figure 5. The plot shows that the terms are not equal. The magnitude of the departure from local isotropy can be quite large, the ratio of the largest to smallest terms in figure 5 being in the range 3 to 1. The smallest terms in (4) are associated with streamwise derivatives. The largest contributions to (4) is due to the spanwise derivative of the spanwise velocity fluctuation, although $\overline{(\partial v/\partial y)^2}$ is only marginally smaller than $\overline{(\partial w/\partial z)^2}$.

The ratios K_1, K_2, K_3 and K_4, ((6) to (9)), are plotted in figure 6(*a*). While K_1 and K_2 are larger than unity, K_3 and K_4 are smaller than unity. This trend is in agreement with the majority of the data in tables 1 and 2. The relative behaviour of the four ratios in figure 6(*a*), when taken in isolation from the other terms in (4), tends to

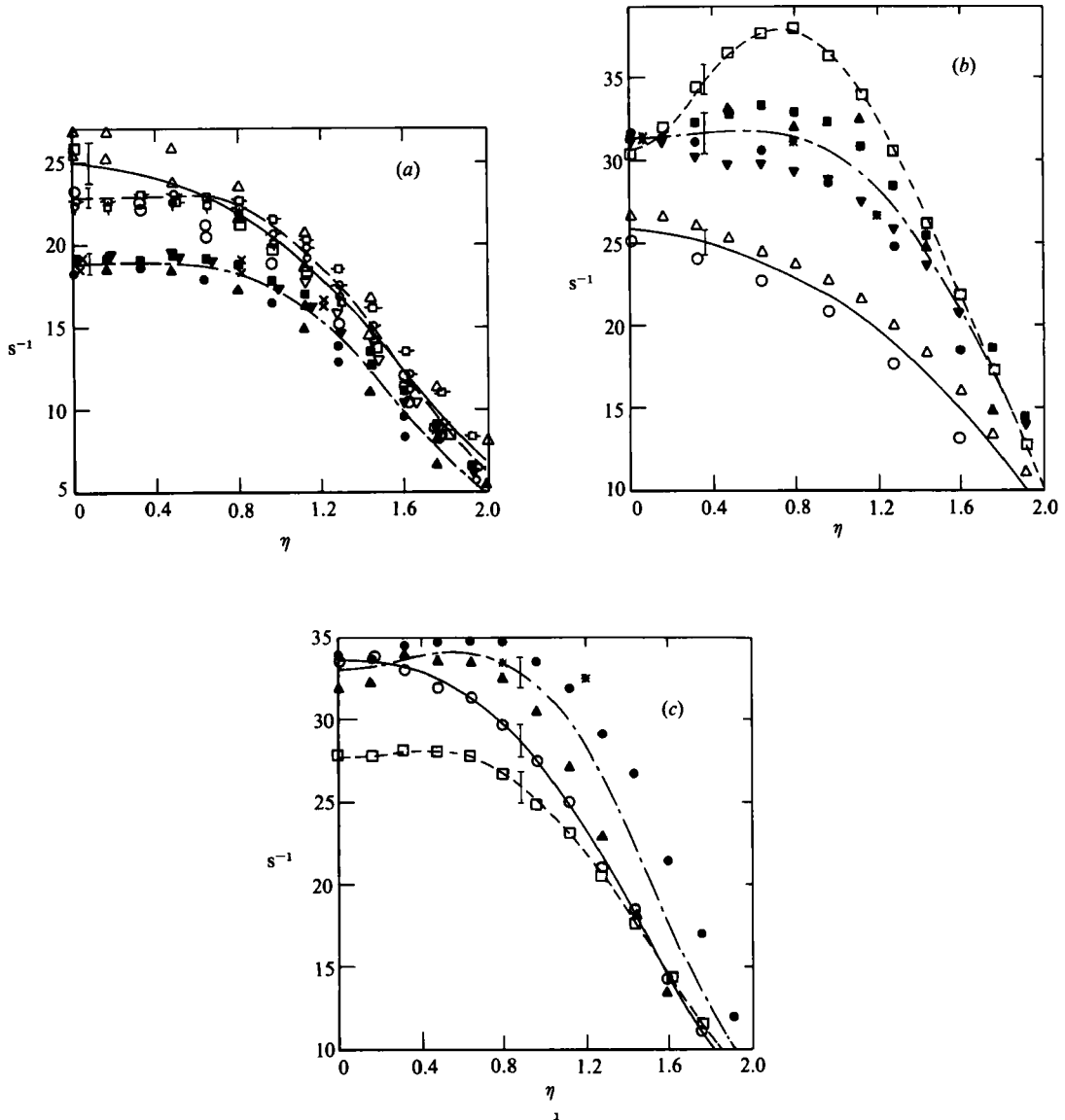

FIGURE 4. Distribution across the wake of $\overline{(\partial\beta/\partial\gamma)^2}^{\frac{1}{2}}$, the r.m.s. of derivatives of velocity fluctuations. Best fit lines: ——, $\beta = u$; ——, v; – – –, w. (*a*) $\gamma = x$: ●, $\beta = u$ (figure 1*a*); ▲, $\beta = u$ (figure 1*a*, repeated); ▼, $\beta = u$ (figure 1*b*); ■, $\beta = u$ (figure 1*c*); ○, $\beta = v$ (figure 1*a*, lower X-wire); △, $\beta = v$ (figure 1*a*, upper X-wire); □, $\beta = v$ (figure 1*d*, X-wire at $z = 0$); ▽, $\beta = v$ (figure 1*d*, X-wire at $z = 1.6$ mm); ⊽, $\beta = w$ (figure 1*b*, lower X-wire); –□–, $\beta = w$ (figure 1*b*, upper X-wire); ⊽, $\beta = w$ (figure 1*c*, X-wire at $z = 0$); –○–, $\beta = w$ (figure 1*c*, X-wire at $z = 1.6$ mm). ×, $\beta = u$, using two single wires. (*b*) $\gamma = y$: ●, $\beta = u$ (figure 1*a*); ▲, $\beta = u$ (figure 1*a*, repeated); ▼, $\beta = u$ (figure 1*a*, repeated); ■, $\beta = u$ (figure 1*b*); ○, $\beta = v$ (figure 1*a*); △, $\beta = v$ (figure 1*a*, repeated); □, $\beta = w$ (figure 1*b*); ★, $\beta = u$, using two single wires. (*c*) $\gamma = z$: ●, $\beta = u$ (figure 1*c*); ▲, $\beta = u$ (figure 1*d*); ○, $\beta = v$ (figure 1*d*); □, $\beta = w$ (figure 1*c*); ★, $\beta = u$, using two single wires.

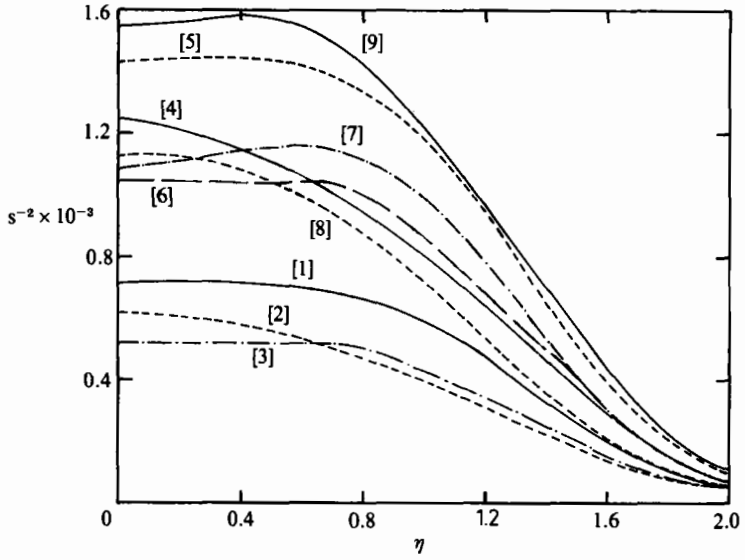

FIGURE 5. Distributions across the wake of terms [1] to [9] of (4).

suggest that some compensation could occur between terms in (4) so that (3) is a reasonable overall approximation to (4). Such a suggestion does not gain support from the ratios K_5 to K_{12}, constructed and defined as follows:

$$K_5 = 2\overline{(\partial v/\partial y)^2}/\overline{(\partial u/\partial y)^2}, \quad K_6 = 2\overline{(\partial v/\partial y)^2}/\overline{(\partial w/\partial y)^2},$$
$$K_7 = 2\overline{(\partial v/\partial y)^2}/\overline{(\partial v/\partial x)^2}, \quad K_8 = 2\overline{(\partial v/\partial y)^2}/\overline{(\partial v/\partial z)^2},$$
$$K_9 = 2\overline{(\partial w/\partial z)^2}/\overline{(\partial u/\partial z)^2}, \quad K_{10} = 2\overline{(\partial w/\partial z)^2}/\overline{(\partial v/\partial z)^2},$$
$$K_{11} = 2\overline{(\partial w/\partial z)^2}/\overline{(\partial w/\partial x)^2}, \quad K_{12} = 2\overline{(\partial w/\partial z)^2}/\overline{(\partial w/\partial y)^2}.$$

With the exception of K_6 and K_{12}, which fall slightly below 1, the remaining ratios are all greater than unity (figures 6*b*, *c*). In particular K_7 and K_{11} show the largest departures from isotropy. It is clear therefore that little compensation, in the sense of validating (3), occurs.

The results obtained for terms [10] and [11] of (4) were poor – the scatter being large and the resulting values tending to fluctuate in sign for separate realizations of the same experiment. Because of the volume occupied by the two probes, phase differences between such quantities as $\partial u/\partial y$ and $\partial v/\partial x$ are likely to degrade the correlation $\overline{(\partial u/\partial y)(\partial v/\partial x)}$. This phase problem does not arise in the case of terms [1] to [9] of (4). Because of the uncertainty in estimating terms [10] and [11], we have assumed the isotropic relation, (5), for these terms as well as for term [12]. In view of the 'expected' smaller values of these three terms compared with the first nine terms in (4), this assumption is unlikely to be critical in our estimate of $\bar{\epsilon}$. The results are shown in figure 7 where it can be seen that the assumption of isotropy, (3), underestimates our approximation for the total dissipation by about 45% on the centreline to about 80% in the outer regions of the wake.

Laufer (1954) assumed that local isotropy may be approximately satisfied by derivatives with respect to a given direction, i.e. $2\overline{(\partial u/\partial x)^2} = \overline{(\partial v/\partial x)^2} = \overline{(\partial w/\partial x)^2}$, and

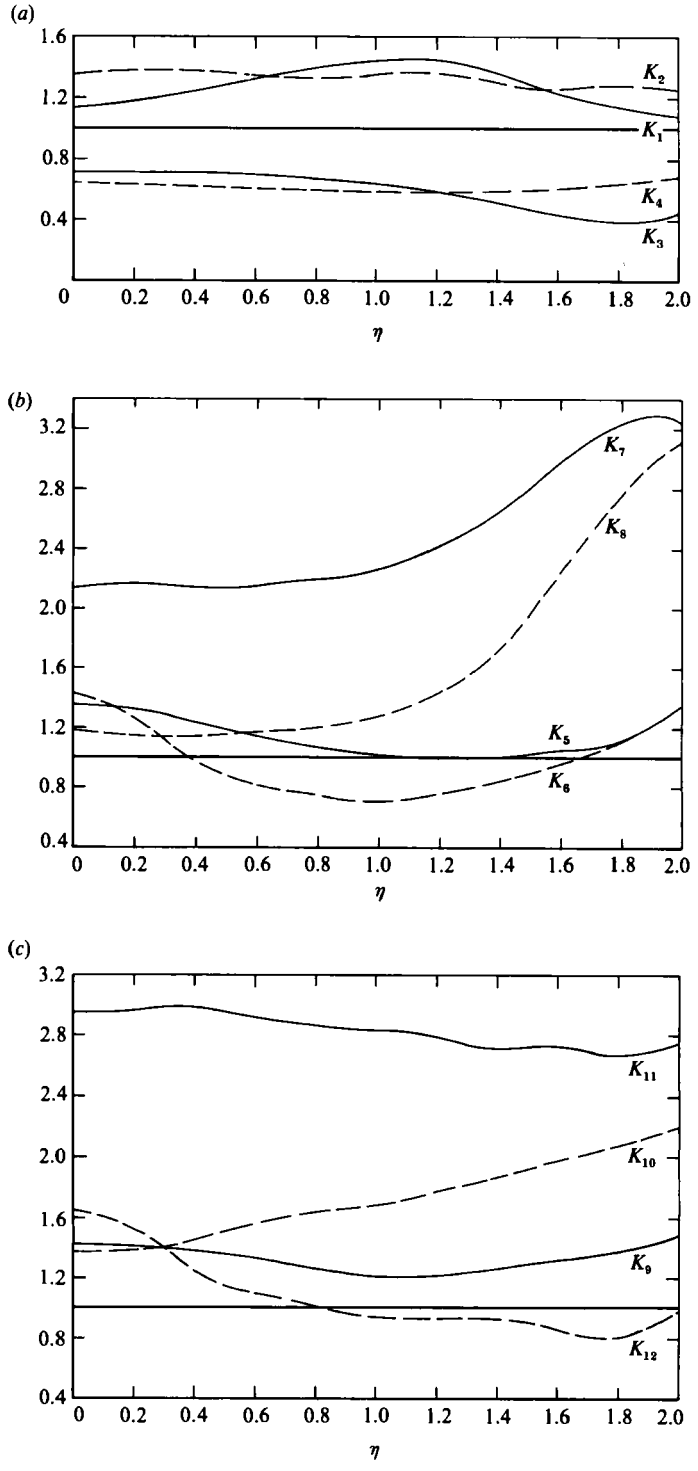

FIGURE 6. Distributions across the wake of ratios K_1 to K_{12}. (*a*) K_1 to K_4; (*b*) K_5 to K_8; (*c*) K_9 to K_{12}. ——, Isotropy value.

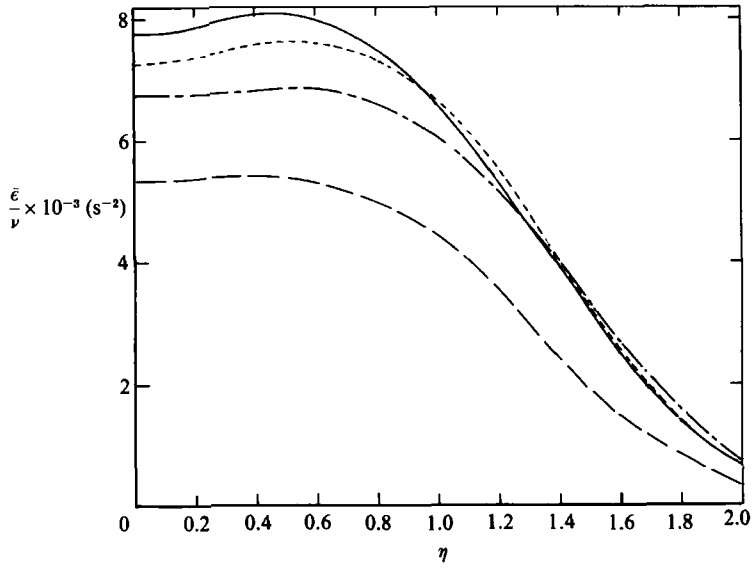

FIGURE 7. Distribution across the wake of different estimates of average dissipations of turbulent energy. ——, $\bar{\epsilon}/\nu$: from experimental results for terms [1] to [9] of (4) and estimates of terms [10] to [12] using (5); — — —, $\bar{\epsilon}_{\mathrm{I}}/\nu$: $15\overline{(\partial u/\partial x)^2}$; – – – –, $\bar{\epsilon}/\nu$: using (14); —·—·—, $\bar{\epsilon}_{\mathrm{SI}}/\nu$: using (15).

similar relations for the other two directions. A reasonable approximation to $\bar{\epsilon}$, assuming also that (5) is valid, would then be

$$\bar{\epsilon} \approx 3\nu\left[\overline{\left(\frac{\partial u}{\partial x}\right)^2}+\overline{\left(\frac{\partial u}{\partial y}\right)^2}+\overline{\left(\frac{\partial u}{\partial z}\right)^2}\right]. \tag{14}$$

This expression represents a semi-isotropic approximation, the basis of which is not rigorously supported by figure 5. We can however take advantage of the compensating effect noticeable in figure 5: whereas $\overline{(\partial u/\partial y)^2}$ or $\overline{(\partial u/\partial z)^2}$ are not the largest terms representing gradients in the y- or z-directions, $2\overline{(\partial u/\partial x)^2}$ is the largest of the first three terms in (4). The agreement between approximation (14) and the distribution for $\bar{\epsilon}$ obtained with (4) and (5) is satisfactory. The estimation of $\bar{\epsilon}$ using (14) is not difficult since only a pair of hot wires is needed to take the required measurements. However, the validity of (14) should be established for other shear flows before it can be claimed as a useful empirical result.

In the context of Laufer's (1954) assumption, Wygnanski & Fiedler (1969) suggested a 'semi-isotropic' approximation for $\bar{\epsilon}$ based on their measurements in a self-preserving circular jet of five terms in (4). Their 'semi-isotropic' expression for dissipation can be written as

$$\bar{\epsilon}_{\mathrm{SI}} \approx \nu\left[\overline{\left(\frac{\partial u}{\partial x}\right)^2}(1+2k)+2\overline{\left(\frac{\partial u}{\partial y}\right)^2}\left(2+\frac{1}{k}\right)\right], \tag{15}$$

where k is obtained from the relation

$$k\overline{\left(\frac{\partial u}{\partial x}\right)^2} = \overline{\left(\frac{\partial v}{\partial x}\right)^2} = \overline{\left(\frac{\partial w}{\partial x}\right)^2}. \tag{16}$$

Expression (15) reduces to expression (3) when k assumes the isotropic value of 2.

Wygnanski & Fiedler found that $\bar{\epsilon}_{\mathrm{SI}}$ was larger than $\bar{\epsilon}_{\mathrm{I}}$ except near the jet

centreline. The present estimates of k obtained using (16) depend, albeit to a small extent, on whether $\overline{(\partial v/\partial x)^2}$ or $\overline{(\partial w/\partial x)^2}$ is used and also the location in the wake (figure 4*a*). The present estimates of $k(\eta)$, typically in the range 1.4–1.8, were obtained using $k(\eta) = [\overline{(\partial v/\partial x)^2} + \overline{(\partial w/\partial x)^2}]/2\overline{(\partial u/\partial x)^2}$. Estimates of $\bar{\epsilon}_{\rm SI}$ were then determined using $k(\eta)$ and relation (15). The ratio of $\bar{\epsilon}$, as obtained with (4) and (5), and $\bar{\epsilon}_{\rm SI}$ varies from 1.15 at the wake centreline to about 0.9 at the edge of the wake (figure 7). The reasonable agreement between $\bar{\epsilon}$ and $\bar{\epsilon}_{\rm SI}$ is encouraging but it should be noted that the determination of $\bar{\epsilon}_{\rm SI}$ requires the use of one X-wire to determine k and also the use of parallel wires to determine $\overline{(\partial u/\partial y)^2}$. Also, as noted for (14), (15) cannot be rigorously validated since the isotropic approximations used to derive (15) are not supported by figure 5. On the basis of the present evidence, (14), which only requires the use of parallel wires for its implementation, seems to provide a better approximation to the $\bar{\epsilon}$ measurements.

5. Average turbulent kinetic energy budget

An approximation to the transport equation for the average turbulent kinetic energy ($\overline{q^2} \equiv \overline{u^2} + \overline{v^2} + \overline{w^2}$) is given by (e.g. Townsend 1949)

$$\underset{\text{advection}}{U_1 \frac{\partial}{\partial x}(\tfrac{1}{2}\overline{q^2})} + \underset{\text{production}}{\overline{uv}\frac{\partial \overline{U}}{\partial y}} + \underset{\text{diffusion}}{\frac{\partial}{\partial y}\overline{v(\tfrac{1}{2}q^2 + p)}} + \underset{\text{dissipation}}{\bar{\epsilon} = 0} \quad . \tag{17}$$

Estimates were made for all the terms in (17) except for the pressure diffusion term which was determined by difference. The gradient $\partial\overline{q^2}/\partial x$ was inferred from the streamwise variations, given in I, of U_0, the centreline defect velocity, and L and the self-preserving form $h(\eta)$ where $\overline{q^2} = U_0^2 h(\eta)$, using

$$\frac{\partial \overline{q^2}}{\partial x} = U_0^2\left(\frac{\mathrm{d}h}{\mathrm{d}\eta}\right)\left(-\frac{\eta}{L}\right)\left(\frac{\mathrm{d}L}{\mathrm{d}x}\right) + 2hU_0\left(\frac{\mathrm{d}U_0}{\mathrm{d}x}\right).$$

A cubic spline least-squares fit was first applied to the data for $\overline{q^2}/U_0^2$. Numerical differentiation of this fit then yielded $\mathrm{d}h/\mathrm{d}\eta$. The lateral derivatives of $\overline{U}$ and $\overline{q^2 v}$ were obtained in similar fashion. The Reynolds shear stress distribution was in reasonable agreement with a calculation, set out and discussed in Browne & Antonia (1986), based on integrating the momentum equation.

Since $\overline{w^2 v}$, one of the three components of $\overline{q^2 v}$, was not measured, some comments regarding the formation of $\overline{q^2 v}$ are required. Since Fabris (1974, 1983) measured all three components of $\overline{q^2 v}$ (with a three-wire probe) at approximately the same flow location and experimental conditions as the present experiment, we first compared our distributions of $\overline{u^2 v}/U_0^3$ and $\overline{v^3}/U_0^3$ with those of Fabris. The comparison was good in the case of $\overline{v^3}/U_0^3$ (figure 8) although the present maximum values of $|\overline{u^2 v}/U_0^3|$ (figure 8) were larger than that of Fabris by nearly 66%. In view of the similarity in the shapes of the $\overline{u^2 v}$ and $\overline{w^2 v}$ distributions (as obtained by Fabris 1974 or Townsend 1949), we inferred our distribution for $\overline{w^2 v}$ from our $\overline{u^2 v}$ data via the relation

$$(\overline{w^2 v})_{\rm present} = (\overline{u^2 v})_{\rm present}\left(\frac{\overline{w^2 v}}{\overline{u^2 v}}\right)_{\rm Fabris}. \tag{18}$$

The resulting values of $\overline{w^2 v}/U_0^3$ are shown in figure 8 with those of Fabris. In general, the magnitude of $\overline{w^2 v}$ is sufficiently smaller than $\overline{u^2 v}$ or $\overline{v^3}$ to suggest that the

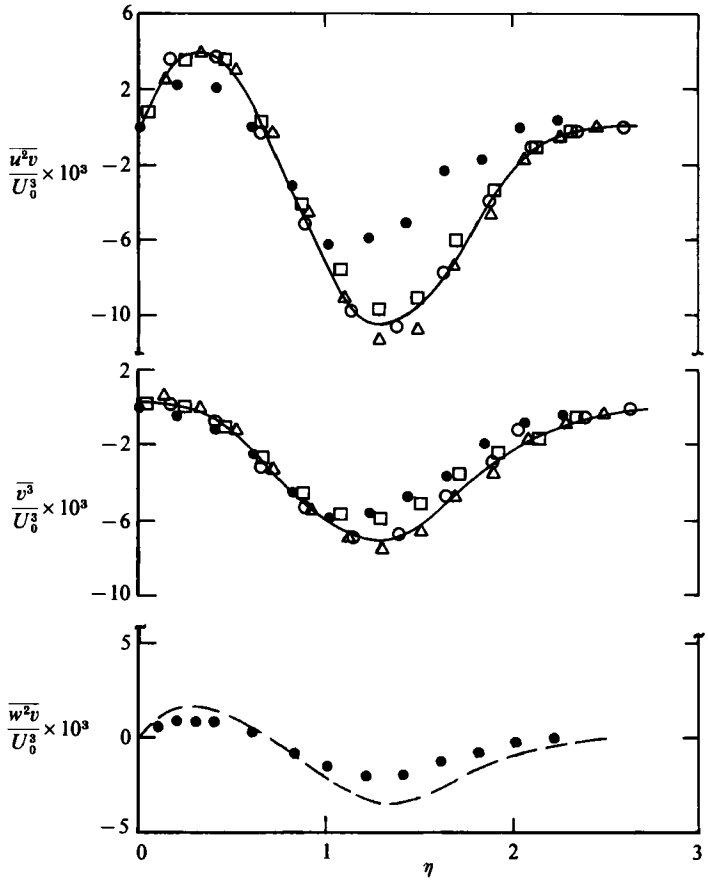

FIGURE 8. Distributions across the wake of the triple velocity products that appear in the diffusion of energy due to lateral velocity fluctuations. △, $x/d = 273$; ○, 420; □, 600: (——, best fit). ●, Fabris (1983), at $x/d = 400$. – – –, present values of w^2v scaled using (18).

determination of $\overline{w^2v}$ is not critical in the context of obtaining $\overline{q^2v}$. Fabris (1983) underlined that the lateral transport of $\overline{u^2}$ and $\overline{v^2}$ is three times as intense as that for $\overline{w^2}$ fluctuations.

The various terms in (17), normalized by multiplying with L/U_0^3, are plotted in figure 9. At the centreline of the wake, the gain of energy due to almost equal contributions from the advection and $\overline{q^2}$ diffusion terms counteracts the loss due to dissipation. As the distance from the axis increases, production and dissipation tend to balance each other but the $\overline{q^2}$ diffusion and advection terms are also approximately equal and of opposite sign. It is interesting that the pressure diffusion term, obtained by difference, is small compared with the diffusion of $\overline{q^2}$. Also, the two diffusion distributions are generally of opposite sign. Assuming symmetry with respect to $\eta = 0$, these distributions satisfy the integral constraints

$$\int_{-\infty}^{\infty} \frac{\partial}{\partial y}(\overline{q^2v})\,\mathrm{d}y = 0,$$

and

$$\int_{-\infty}^{\infty} \frac{\partial}{\partial y}(\overline{pv})\,\mathrm{d}y = 0,$$

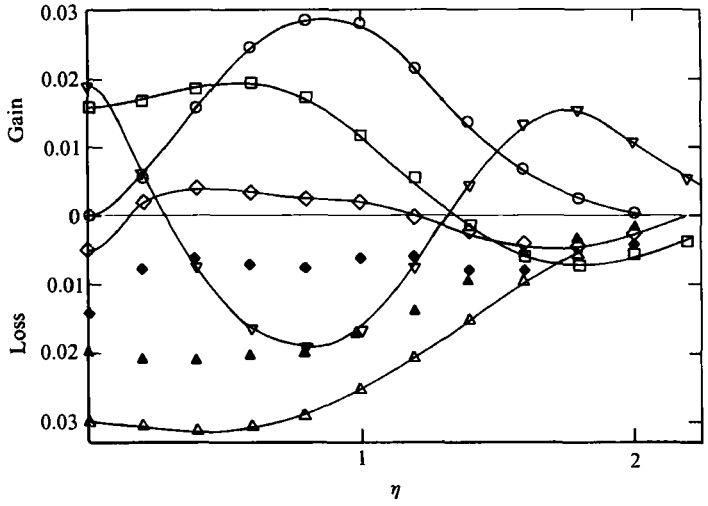

FIGURE 9. Measured budget of average turbulent energy. ○, production; □, advection; ▽, q^2 diffusion; △, dissipation, $\bar{\epsilon}$, equations (4) and (5); ◇, pressure diffusion (by difference). ▲, isotropic dissipation, equation (3); and ◆, corresponding pressure diffusion. Values normalized by L/U_0^3.

by about 2% and 8% respectively. If the isotropic dissipation $\bar{\epsilon}_I$ was used instead of $\bar{\epsilon}$, the resulting pressure diffusion would retain the same sign throughout the wake, see figure 9, thereby violating the above integral constraint. This demonstrates that, at least in the present case, the $\partial/\partial y\,(\overline{pv})$ distribution will be inaccurate if isotropy is assumed.

The present pressure diffusion distribution contrasts strongly with that obtained by Townsend (1949) in the far field of a cylinder wake at $R_d = 8400$. Townsend assumed isotropy to determine the dissipation, after verifying that $K_1 \approx K_2 \approx 1$ (Townsend 1948). The resulting pressure diffusion, obtained by difference, was generally unrealistically high, of the same order as production and dissipation near the region of maximum production. Although Townsend's $\overline{q^2}$ diffusion satisfied the integral constraint approximately, his pressure diffusion did not. The reason for this is probably that, despite the relatively high Reynolds number, the estimation of $\bar{\epsilon}$ was inaccurate due to the assumption of local isotropy.

It should also be noted that a direct estimate of the pressure diffusion was made by Kobashi (1957) for a cylinder wake. Reservations have been expressed with regard to these measurements (e.g. Hinze 1975 p. 514) and it is evident that they may not be directly relevant to the present study since they were made at a distance of only 40 diameters from the cylinder (the distributions of energy diffusion and advection differ significantly from those in the self-preserving region). Nevertheless, the two diffusion distributions obtained by Kobashi satisfy approximately the integral constraints, and the magnitude of the pressure diffusion was generally smaller than that of the energy diffusion.

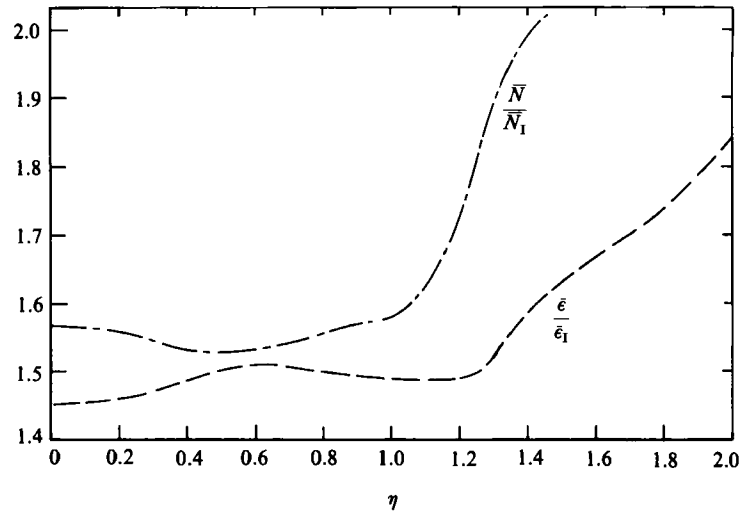

FIGURE 10. Distributions across the wake of ratios of the total and isotropic dissipations of ----, the average turbulent energy and ——— temperature variance.

6. Comparison between average dissipations of turbulent energy and temperature variance

In I, measurements were presented, for the same flow and conditions as investigated here, of the average temperature dissipation, $\overline{N}$, at this same station. Denoting by θ the temperature fluctuation and by α the thermal diffusivity, then

$$\overline{N} = \alpha\left[\overline{\left(\frac{\partial\theta}{\partial x}\right)^2} + \overline{\left(\frac{\partial\theta}{\partial y}\right)^2} + \overline{\left(\frac{\partial\theta}{\partial z}\right)^2}\right]. \tag{19}$$

Assuming isotropy, the average temperature dissipation is given by

$$\overline{N}_I = 3\alpha\overline{\left(\frac{\partial\theta}{\partial x}\right)^2}. \tag{20}$$

The ratio $\overline{N}/\overline{N}_I$, as obtained in I, has been included in figure 10 for comparison with the present distribution of $\bar{\epsilon}/\bar{\epsilon}_I$. There is an interesting similarity between these two ratios. In particular, there is relatively little variation between the centreline and $\eta = 1$, although the gentle peak of $\bar{\epsilon}/\bar{\epsilon}_I$ at $\eta \approx 0.6$ corresponds approximately with a gentle dip in $\overline{N}/\overline{N}_I$. Both $\overline{N}/\overline{N}_I$ and $\bar{\epsilon}/\bar{\epsilon}_I$ increase near the wake edge although the increase in $\overline{N}/\overline{N}_I$ is steeper and occurs at a smaller η than that for $\bar{\epsilon}/\bar{\epsilon}_I$. Notwithstanding the general difficulty (e.g. Antonia *et al.* 1986) of comparing fine-scale velocity and temperature fields, an interesting similarity seems to exist between the relative magnitude of the components of $\overline{N}$ and those of $\bar{\epsilon}$. An uncertainty analysis for $\bar{\epsilon}/\bar{\epsilon}_I$, using as uncertainties in individual values the r.m.s. of the scatter of the data shown in figure 4, gave an error range of about $\pm 6\,\%$ for $\eta = 0$ to 1.2. A similar result holds for the $\overline{N}/\overline{N}_I$ curve so that the two curves are in fact very similar, at least up to $\eta = 1.2$.

It has now been established (see e.g. I; Verollet 1972), for many different flows that $\overline{(\partial\theta/\partial z)^2}$ and $\overline{(\partial\theta/\partial y)^2}$ are almost equal in magnitude but significantly larger than $\overline{(\partial\theta/\partial x)^2}$. A similar inequality applies between mean-squared values of velocity

derivatives in either the z- or y-direction and those in the x-direction. Spectra of $\partial\theta/\partial y$ or $\partial\theta/\partial z$ have appreciably larger low-frequency contents compared with the spectrum of $\partial\theta/\partial x$ (e.g. Sreenivasan, Antonia & Danh 1977). A similar relative behaviour has been obtained between spectra of $\partial u/\partial y$ or $\partial u/\partial z$ and the spectrum of $\partial u/\partial x$ (Antonia *et al.* 1984). We have established during this investigation that this relative behaviour extends to fluctuations v and w. Quantities such as $\overline{(\partial\beta/\partial y)^2}$ and $\overline{(\partial\beta/\partial z)^2}$, where $\beta \equiv u, v, w$, are more likely to be affected by the anisotropy of the large-scale motion than $\overline{(\partial\beta/\partial x)^2}$. This suggests that the inequality between the x-, y- and z-derivatives, as they appear in (4), is consistent with the results obtained from temperature measurements.

7. Concluding discussion

The present measurements, in a low-Reynolds-number cylinder wake, have confirmed previously published departures from isotropy of the ratios $\overline{(\partial v/\partial x)^2}/\overline{(\partial u/\partial x)^2}$, $\overline{(\partial w/\partial x)^2}/\overline{(\partial u/\partial x)^2}$, $\overline{(\partial u/\partial y)^2}/\overline{(\partial u/\partial x)^2}$ and $\overline{(\partial u/\partial z)^2}/\overline{(\partial u/\partial x)^2}$ or their inverse, in different turbulent shear flows and Reynolds numbers. The corresponding ratios for the terms $\overline{(\partial v/\partial y)^2}$, $\overline{(\partial w/\partial y)^2}$, $\overline{(\partial v/\partial z)^2}$, $\overline{(\partial w/\partial z)^2}$, which have not been previously measured in the literature, also exhibit significant departures from isotropy. The departure from isotropy of the major terms in (4) is such that the isotropic dissipation, given by (3), is inadequate. Overall the use of $15\nu\overline{(\partial u/\partial x)^2}$, at least in the present flow, underestimates the measured dissipation by almost 45 % at the centreline, where the flow is fully turbulent, and by 80 % near the edge of the wake, where the effect of intermittency becomes important.

Some support for the accuracy of the measurements of $\bar{\epsilon}$ is provided by the budget of the average turbulent energy. The closure for this budget is reasonable in that the terms representing transport of the turbulent energy by velocity and pressure fluctuations integrate approximately to zero across the wake. The magnitude of the pressure transport term is small compared with other terms in the budget.

The Reynolds number of the present experiment is too small (e.g. no inertial subrange can be found in the spectra of u, v or w) to expect local isotropy to apply. In this sense, it may be argued that the measured anisotropy of the average turbulent energy dissipation is not surprising. The information in tables 1 and 2 shows however that the departure from isotropy of the ratios K_1–K_4, which are formed using five components of $\bar{\epsilon}$, does not seem to depend on the Reynolds number. It is therefore unlikely that the anisotropy of $\bar{\epsilon}$ is restricted only to the present flow and Reynolds number.

At this stage we can only speculate on the applicability of the present results to other shear flows and Reynolds numbers. Antonia *et al.* (1986) noted that one factor which has made it difficult to interpret fine-scale measurements in the context of isotropy, is the possible contamination of these measurements by the anisotropic large-scale motion. There is now sufficient evidence of the existence of a relatively organized large-scale motion in a wide range of non-homogeneous turbulent shear flows. The presence of large-scale vortical bulges in the present flow has been well documented and the topology of the motion associated with these bulges has been described by Browne, Antonia & Bisset (1986) and Antonia *et al.* (1987). In the latter paper, it was suggested that each bulge comprised vortex loops or hairpin vortices whose planes lie at approximately 45° to the flow direction, in approximate alignment with the direction of the principal rate of strain. There is evidence (e.g. Antonia *et al.* 1986) to suggest that the dissipation of turbulent energy (or temperature variance)

will be concentrated along this direction, thus providing an intimate link between the anisotropy of the large-scale motion and the anisotropy of the dissipation. Although the degree of organization may vary from flow to flow and with the Reynolds number, the presence of the (anisotropic) large-scale motion is not in question, thus providing a plausible extension for the validity of the present results to other non-homogeneous shear flows and Reynolds numbers. Using a database generated by direct numerical solution of the Navier–Stokes equations for homogeneous turbulence in the presence of uniform shear, Moin, Rogers & Moser (1985) noted the existence of hairpin vortices, a result also obtained (Moin & Kim 1985) when the same technique was applied to a turbulent channel flow. These authors asserted that hairpin vortices are the dominant structures in all shear flows. The anisotropy of the energy and temperature dissipations observed in the measurements of Tavoularis & Corrsin (1981) in a homogeneous turbulent shear flow lends support to the suggestion that the validity of the present results may be extended to *all* shear flows. It will be useful, in future work, to determine quantitative measures for the anisotropy of the organized motion in different shear flows and Reynolds numbers.

With due allowance for the previous speculative remarks the present results have important implications: since the majority of turbulent energy budgets in the literature have been based on isotropy, they are likely to be in error and conclusions about the pressure diffusion term can only be viewed with reservation. Similarly, any computer models that use estimates of the turbulent energy dissipation based on isotropy, are likely to be in error.

The support of the Australian Research Grants Scheme is gratefully acknowledged.

REFERENCES

ANTONIA, R. A., ANSELMET, F. & CHAMBERS, A. J. 1986 Assessment of local isotropy using measurements in a turbulent plane jet. *J. Fluid Mech.* **163**, 365–391.

ANTONIA, R. A., BROWNE, L. W. B., BISSET, D. K. & FULACHIER, L. 1987 Topology of the organized motion in the turbulent far-wake of a cylinder. *J. Fluid Mech.* (submitted).

ANTONIA, R. A. & BROWNE, L. W. B. 1986 Anisotropy of the temperature dissipation in a turbulent wake. *J. Fluid Mech.* **163**, 393–403.

ANTONIA, R. A., BROWNE, L. W. B. & CHAMBERS, A. J. 1984 On the spectrum of the transverse derivative of the streamwise velocity in a turbulent flow. *Phys. Fluids* **27**, 2628–2631.

ANTONIA, R. A., RAJAGOPALAN, S., BROWNE, L. W. B. & CHAMBERS, A. J. 1982 Correlations of squared velocity and temperature derivatives in a turbulent plane jet. *Phys. Fluids* **25**, 1156–1158.

BATCHELOR, G. K. 1953 *The Theory of Homogeneous Turbulence.* Cambridge University Press.

BROWNE, L. W. B. & ANTONIA, R. A. 1986 Reynolds shear stress and heat flux measurements in a cylinder wake. *Phys. Fluids* **29**, 709–713.

BROWNE, L. W. B., ANTONIA, R. A. & BISSET, D. K. 1986 Coherent structures in the far-field of a turbulent wake. *Phys. Fluids* **29**, 3612–3617.

CHAMPAGNE, F. H. 1978 The fine-scale structure of the turbulent velocity field *J. Fluid Mech.* **86**, 67–108.

CHAMPAGNE, F. H., PAO, Y. H. & WYGNANSKI, I. J. 1976 On the two-dimensional mixing region. *J. Fluid Mech.* **74**, 209–250.

EVERITT, K. W. & ROBINS, A. G. 1978 The development and structure of turbulent plane jets. *J. Fluid Mech.* **88**, 563–583.

FABRIS, G. 1974 Conditionally sampled turbulent thermal and velocity fields in the wake of a warm cylinder and its interaction with an equal cool wake. Ph.D. thesis, Illinois Institute of Technology.

FABRIS, G. 1983 Third-order conditional transport correlations in the two-dimensional turbulent wake. *Phys. Fluids* **26**, 422–427.

GUTMARK, E. & WYGNANSKI, I. 1976 The planar turbulent jet. *J. Fluid Mech.* **73**, 465–495.

HINZE, J. O. 1975 *Turbulence*. McGraw-Hill.

JEFFREYS, H. 1963 *Cartesian Tensors*. Cambridge University Press.

KOBASHI, Y. 1957 Measurements of pressure fluctuation in the wake of a cylinder. *J. Phys. Soc. Japan* **12**, 533–543.

KRISHNAMOORTHY, L. V. & ANTONIA, R. A. 1987 Temperature-dissipation measurements in a turbulent boundary layer. *J. Fluid Mech.* **176**, 265–281.

LAUFER, J. 1954 The structure of turbulence in fully developed pipe flow. *NACA Rep.* 1174.

LAWN, C. J. 1971 The determination of the rate of dissipation in turbulent pipe flow. *J. Fluid Mech.* **48**, 477–505.

MOIN, P. & KIM, J. 1985 The structure of the vorticity field in turbulent channel flow. Part 1. Analysis of instantaneous fields and statistical correlations. *J. Fluid Mech.* **155**, 441–464.

MOIN, P., ROGERS, M. M. & MOSER, R. D. 1985 Structure of turbulence in the presence of uniform shear. *Proc. Fifth Symp. on Turbulent Shear Flows, Cornell University*, pp. 17.21–17.26.

NELKIN, M. & NAKANO, T. 1984 How do the small scales become isotropic in Navier–Stokes turbulence. In *Turbulence and Chaotic Phenomena in Fluids* (ed. T. Tatsumi), pp. 319–323. North-Holland.

SREENIVASAN, K. R., ANTONIA, R. A. & DANH, H. Q. 1977 Temperature dissipation fluctuations in a turbulent boundary layer. *Phys. Fluids* **20**, 1238–1249.

TAVOULARIS, S. & CORRSIN, S. 1981 Experiments in nearly homogeneous turbulent shear flow with a uniform mean temperature gradient. Part 1. *J. Fluid Mech.* **104**, 311–347.

TAYLOR, G. I. 1935 Statistical theory of turbulence. Parts 1–4. *Proc. R. Soc. Lond.* A **151**, 421–478.

TOWNSEND, A. A. 1948 Local isotropy in the turbulent wake of a cylinder. *Austral. J. Sci. Res.* **1**, 161–174.

TOWNSEND, A. A. 1949 The fully developed turbulent wake of a circular cylinder. *Austral. J. Sci. Res.* **2**, 451–468.

VEROLLET, E. 1972 Etude d'une couche limite turbulente avec aspiration et chauffage à la paroi. Thèse Docteur ès Sciences, Université de Provence. (Also Rapport CEA-R-4872, CEN Saclay).

WYGNANSKI, I. & FIEDLER, H. 1969 Some measurements in the self-preserving jet. *J. Fluid Mech.* **38**, 577–612.

WYNGAARD, J. C. 1968 Measurement of small scale turbulence structure with hot wires. *J. Sci. Instrum.* **1**, 1105–1108.